Revista Internacional de Ciencia y Tecnología de la Información Geográfica
International Review of Geographical Information Science and Technology

Navarro-Planes, M. (2026). Trend assessment of snow persistence in the Pyrenees based on Landsat imagery. *GeoFocus*, *Revista Internacional de Ciencia y Tecnología de la Información Geográfica* (Articles), 37, 17-43. https://dx.doi.org/10.21138/GF.962

TREND ASSESSMENT OF SNOW PERSISTENCE IN THE PYRENEES BASED ON LANDSAT IMAGERY

[1,2]Martí Navarro-Planes
[1]Institute of Environmental Assessment and Water Research (IDAEA-CSIC), Barcelona, Spain
[2]Grumets Research Group, Department of Geography, Building B, Universitat Autònoma de Barcelona, 08193 Bellaterra, Catalonia, Spain
mnphse@cid.csic.es

ABSTRACT

A precise quantification of the spatio-temporal dynamics of snow cover is essential to assess the impact of climate change on mountain ecosystems, particularly in mid-mountain regions of southern Europe such as the Pyrenees. This study analyses the evolution of Snow Persistence (SP), defined as the fraction of time that snow remains on the ground, from 1984 to 2024 in the main river basins of the western Catalan Pyrenees. The analysis is based on remote sensing techniques using historical Landsat time series, with snow cover identified through the Normalized Difference Snow Index (NDSI). The results reveal a decline in SP across 73 % of the study area, indicating a transition from permanent winter snow cover to a more intermittent snow regime. Snow line elevation shows that seasonal snow cover during the 2014-2024 decade was located, on average, 267 m higher than during the 1984-1994 decade. The multiple regression model including altitude and solar irradiation explained 47.4 % of the spatial variability in SP, with a positive effect of altitude and a negative effect of solar radiation. Despite some methodological limitations, mainly related to temporal resolution and radiometric inconsistencies in Landsat Collection 2 Level 2 images, the results provide robust evidence of significant changes in snow dynamics.

Keywords: snow persistence; snow cover; remote sensing; Landsat; NDSI.

EVALUACIÓN DE TENDENCIAS DE LA PERSISTENCIA DE LA NIEVE EN LOS PIRINEOS BASADA EN IMÁGENES LANDSAT

RESUMEN

Una cuantificación precisa de la dinámica espaciotemporal de la cubierta nival es esencial para evaluar el impacto del cambio climático en los ecosistemas de montaña, especialmente en regiones de media montaña del sur de Europa como los Pirineos. Este estudio analiza la evolución de la Persistencia de la Nieve (SP), definida como la fracción de tiempo que permanece en el suelo, entre 1984 y 2024 en las cuencas hidrográficas del Pirineo occidental catalán. El análisis se basa en técnicas de teledetección a partir de series temporales de Landsat, con la cubierta nival identificada mediante el Índice de

Received: 17/02/2026
Accepted: 22/07/2026
Academic Editor: Dr. Miquel Ninyerola
www.geofocus.org
Attribution-NonCommercial-NoDerivatives 4.0 International (CC BY-NC-ND 4.0)

Diferencia Normalizada de Nieve (NDSI). Los resultados muestran un descenso de la SP del 73 % del área de estudio, indicando una transición de una cubierta de nieve hibernal permanente hacia un régimen nival más intermitente. El análisis de la altitud de la línea de nieve indica que la cubierta nival estacional durante la década 2014-2024 se sitúa, en promedio, 267 m por encima de la registrada en la década1984-1994. El modelo de regresión múltiple que incluye la altitud y la radiación solar explica el 47.4 % de la variabilidad espacial de la SP, con un efecto positivo de la altitud y un efecto negativo de la radiación solar. A pesar de algunas limitaciones metodológicas relacionadas con la resolución temporal y con inconsistencias en la corrección radiométrica de las imágenes "Landsat Collection 2 Level 2", los resultados aportan evidencias sólidas de cambios en la dinámica de la nieve.

Palabras clave: persistencia de nieve; cubierta nival; teledetección; Landsat; NDSI.

1. Introduction

The presence or absence of snow in a landscape regulates the land surface energy budget, influences hydrological responses, and affects ecosystem function. An intermittent snow regime, whereby snow does not persist throughout the winter, increases soil exposure to solar irradiance. This results in soil moisture loss through evapotranspiration (Moore *et al.* 2015), limited runoff generation, and reduced soil infiltration during the melt period. Moreover, intermittent melt events can enhance nutrient and carbon leaching from soils to downstream ecosystems by increasing the frequency of freeze–thaw and wet–dry cycles (Brooks & Williams 1999, Wipf *et al.* 2015). These fluctuations stimulate microbial activity and organic matter decomposition, ultimately altering nutrient availability and biogeochemical cycles at the catchment scale. In contrast, a persistent snow cover acts as a protective layer for the soil and local biota, serves as a barrier against nutrient deposition, and promotes greater runoff and soil infiltration during spring (Anenberg 2019). Together, these processes highlight the need for detailed quantification of snow cover dynamics as a basis for assessing the hydrological, ecological, and biogeochemical implications of climate change in seasonally snow-covered mountain landscapes.

Recent research has documented a decline in snow cover extent and a reduction in the duration of the snow season across the Northern Hemisphere (Hammond *et al.* 2018, Hori *et al.* 2017, Robinson *et al.* 2015), with the onset of spring snowmelt occurring progressively earlier in the year (Choi *et al.* 2010). These changes are expected to be particularly pronounced in mid-mountain regions of southern Europe. The Pyrenees, located at the transition between Atlantic and Mediterranean climatic influences, constitute a paradigmatic example of mountains undergoing rapid changes in environmental conditions (Morán-Tejeda *et al.* 2017). The climate of the Pyrenees shows strong east-west variability, as well as marked contrasts between the northward and southward slopes along the main axis of the range, with the former being markedly more humid (López-Moreno *et al.* 2020). The temperatures in the Pyrenees between 1981 and 2020 have shown a significant increase, with an annual trend of +0.26°C per decade. Annual precipitation in the region shows a declining trend, decreasing by 1.4 % per decade (Cuadrat *et al.* 2024).

The combination of rising temperatures and declining precipitation is directly altering the snow regime of the range, particularly in its southern and Mediterranean sectors. As a result, the extent of areas with persistent snow in the southern and Mediterranean sectors of the Pyrenees is decreasing rapidly, with potential impacts on the availability and quality of water resources. A decline in snow cover duration and average snow accumulation was observed between 1958 and 2017 (López-Moreno *et al.* 2020). A recent study conducted at the scale of the entire Pyrenean range reported a reduction in the snow melt-out date (SMOD), defined as the first day with no snow cover, revealing a widespread trend toward earlier snow disappearance, with an average advance of 4.04 days per decade in the Pyrenees (Barrou Dumont *et al.* 2024, Dumont 2025).

The study of snow cover has traditionally relied on in situ observations, which involve inherent risks and logistical challenges. In contrast, remote sensing techniques provide a broader view of the territory, safe access to remote areas, continuous monitoring, and high efficiency in terms of time and resources. Snow can be readily identified under clear-sky conditions due to its high reflectance in the visible spectrum, while its low reflectance in the short-wave infrared (SWIR) allows for effective discrimination from clouds, which are highly reflective at these wavelengths (Cea *et al.* 2007, Dozier 1989). In this study, Landsat imagery was used due to its suitable spectral configuration and the availability of a long and consistent time series.

The objective of this study is to quantify the spatiotemporal dynamics of snow cover in the Catalan Western Pyrenees between March 1984 and March 2024 using satellite imagery. Specifically, the study analyzes long-term changes by first assessing the annual snow-covered area across the entire Landsat time series and then examining snow persistence (SP), defined as the fraction of time that snow remains on the ground. Finally, changes in SP are compared between decades, and their relationships with altitude and solar irradiance are explored.

2. Material and methods

2.1. Study Area

The main study area comprised the river basins of the western Catalan Pyrenees, corresponding to Landsat path 198 and rows 030 and 031. Within these basins, the Aigüestortes i Estany de Sant Maurici National Park allowed a more detailed analysis of SP in relation to environmental variables such as solar irradiance (Figure 1). The western Catalan Pyrenees include the catchments of the Garona (A), Noguera Ribagorçana (B), Noguera Pallaresa (C), Valira (D), and Segre (E) rivers (Figure 1), covering a total area of 4963.24 km² with an altitudinal range of 498 m to 3404 m at Aneto peak. The study area lies almost entirely within Catalonia, with small portions in Aragon, the French Pyrenees, and including the entire territory of Andorra. Hereafter, this area is referred to as “the western Catalan Pyrenees”.

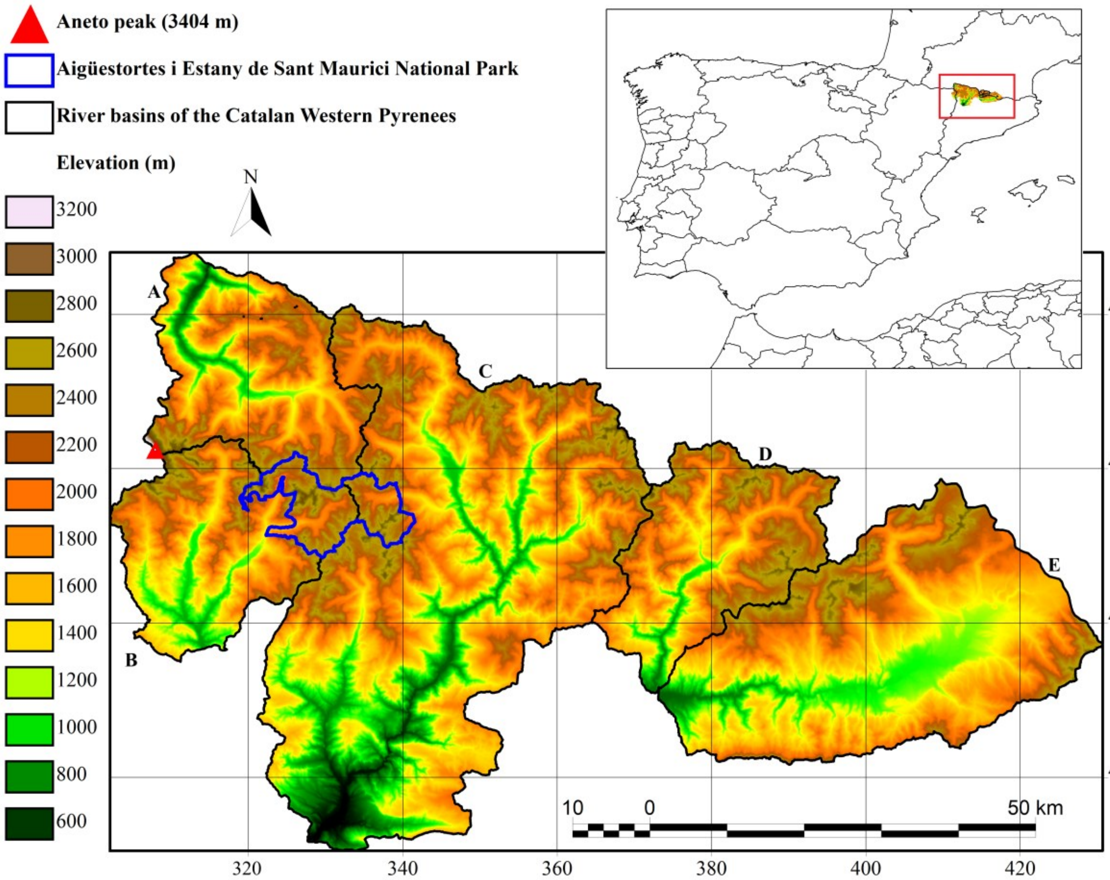

Figure 1. Location map of the study area

Source: own elaboration based on the 30 m terrain elevation model (NASADEM). The main working area is the river basins of the western Catalan Pyrenees. Secondary scale: Aigüestortes i Estany de Sant Maurici National Park. UTM-31N projection; coordinates in km

Vegetation at lower elevations is dominated by Scots pine (*Pinus sylvestris*) and silver fir (*Abies alba*), while mountain pine (*Pinus uncinata*) and alpine rose (*Rhododendron ferrugineum*) are characteristic of the subalpine zone. At higher altitudes, alpine meadows and sparse plant communities adapted to rocky, wind-exposed environments prevail. The terrain is rugged, primarily composed of igneous rocks such as granite, but also includes slate, schist, and limestone. The landscape is shaped by numerous rivers, waterfalls, glacial valleys, and a high density of mountain lakes and ponds.

The Aigüestortes i Estany de Sant Maurici National Park (hereafter "the National Park") is in northwest Catalonia and is the only area in the region with this level of protection, officially declared a National Park on October 21st, 1955. The Park covers 139 km², with elevations ranging from 1300 m to 3013 m (Figure A.1). The National Park scale is used only for the final analysis of SP and solar irradiance, because high-resolution data are available for this protected area (*see section 2.6.4 and 3.6*).

2.2. Remote sensing data

The Landsat platform was chosen due to its 40-year temporal record, high spatial resolution of 30 m, and the ease with which scenes could be downloaded. Satellite images from Landsat missions 4 through 9 covering the study area (path 198, rows 030 and 031) were downloaded from the United States Geological Survey (USGS) portal: https://earthexplorer.usgs.gov/. The scenes belong to Collection 2, level 2, and have already been atmospherically corrected (Pons *et al.* 2025). Scenes from Landsat-1, 2, and 3 were excluded due to differences in spatial resolution and lower temporal frequency. A total of approximately 1800 scenes were processed, which, after being mosaicked along the path, resulted in 903 final images in total. For Landsat-4 to Landsat-9, the decision to work with level 2 scenes was made after testing radiometric corrections on several level 1 Landsat images and evaluating both the results and the processing costs. Due to the high number of 'NoData' pixels (*e.g.*, in northern exposures receiving only diffuse solar irradiance) and the complexity of the correction process, the use of level 1 images was discarded.

For Landsat-4, Landsat-5, and Landsat-7, Surface Reflectance (SR) products were used, generated with the LEDAPS (Landsat Ecosystem Disturbance Adaptive Processing System) software (Sayler 2021). For Landsat-8 and Landsat-9, Surface Reflectance products were also used, but generated using a different algorithm: LaSRC (Land Surface Reflectance Code) (Sayler 2023). LEDAPS laid the groundwork for atmospheric correction and radiometric calibration of Landsat data. However, LaSRC represents a significant advancement, featuring tailored algorithms optimized for Landsat-8 and 9 sensors. Overall, LaSRC provides more accurate and reliable surface reflectance estimates than LEDAPS. Additionally, the potential use of the "Snow cover" quality bands from the Landsat Level 2 product was evaluated. However, in the snow product provided by the USGS there is considerable confusion between clouds and snow, and it includes many areas with missing data, especially in regions affected by strong shadows or cloud cover. Consequently, this product was discarded.

2.3. Satellite image processing and snow cover estimation

The available scenes were imported into the MiraMon software environment (Pons 2004) for further processing. During import, the TIFIMG module automatically applied the scaling factors to all radiometric bands. At this stage, the two scene rows (030 and 031) were mosaicked and clipped to include only the study area.

Next, the normalized difference snow index (NDSI) was computed using the green and SWIR-1 bands to automatically detect snow following the method described by Dozier (1989). The NDSI is widely used to assess the temporal and spatial distribution of snow cover (Dietz *et al.* 2012, Girona-Mata *et al.* 2019) or estimate fractional snow cover (Gascoin *et al.* 2020, Salomonson & Appel 2004). Snow is highly reflective in the visible and near-infrared (NIR) regions of the spectrum, but its reflectance progressively decreases towards the SWIR, where it becomes very low due to snow's strong absorption of radiation at these wavelengths. Because NDSI is a normalized index, it reduces the influence of high reflectance values in SWIR-1 relative to the green band, thus helping to distinguish snow from bright rocks and clouds. The resulting raster of NDSI values ranges from –1 to +1.

In the present study, we applied a fixed NDSI threshold of about 0.4 for snow detection, following Dozier (1989) and Hall & Riggs (2007). Pixels with NDSI ≥ 0.4 were classified as snow, and those with NDSI < 0.4 as no snow. However, the applicability of this canonical threshold at local and mountainous scales has been questioned (Härer *et al.* 2018). Published thresholds vary widely (approximately 0.18 to 0.70) depending on terrain, snow, solar illumination, and vegetation conditions. Other authors, such as Girona-Mata *et al.* (2019) and Zhang *et al.* (2019), use more flexible thresholds depending on regional and environmental factors, or even propose different thresholds depending on whether the area is forested (0.1 < NDSI < 0.4) or not (Painter *et al.* 2009).

2.4. Estimation and elimination of projected shadows

Using Landsat Level 2 images that have been atmospherically corrected with different algorithms for Landsat 4-5-7 and Landsat 8-9 images makes it difficult to compare decades. Classified snow from Landsat 4-5-7 images contained many commission errors in topographically projected shadows, particularly in low-lying areas which are not usually covered by snow. Conversely, classified snow from Landsat 8-9 images contained significant omission errors due to the presence of NoData pixels in the shorter wavelength bands.

To eliminate the effect of topographic shadows when comparing data from different decades, the projected shadows for 21 December were calculated, when the solar height is at its minimum and shadows are at their maximum. This was achieved using the Ombra tool in MiraMon and the NASADEM Digital Elevation Model. The result is a raster in which each pixel shows the minimum solar height required for the pixel to be illuminated by the sun. Using the Astres tool, the solar azimuth and height at the time of the winter solstice were calculated. The results show that, at 10:30 a.m. on 21 December, when the satellite passes over the centre of the study area, the solar azimuth is 155.25 degrees and height is 23.69 degrees. Areas above this angle were discarded, *i.e.* areas requiring a higher solar altitude to avoid shade at this time of day.

This approach ensures that the snow persistence analysis is carried out on areas that are effectively illuminated and avoids errors derived from differences in the radiometric corrections of Landsat Level 2 in areas with projected topographic shadow.

2.5. Satellite image selection

To select images based on cloud cover, an RGB composite of the NIR, SWIR-1, and red bands was created. This produced "Quick-Look" visualizations for all Landsat images, where snow is highlighted in a magenta colour, easily distinguishable from other surfaces. The 903 downloaded images were automatically converted in this RGB composite through JPEGIMG, and visually analysed one by one. A table was created indicating the percentage of cloud cover to the entire scene (mosaicked and clipped to the same limits as the study area) and types of cloud cover (cirrus, cumulus, and stratus) for each date. This allowed us to analyse of the temporal series based on cloud cover thresholds. Finally, it was decided to accept those dates with a cloud cover below 25 %. Out of the initial 903 dates, 500 were accepted.

2.6. Data analysis

2.6.1. Snow cover time series

The snow cover time series was analysed using RStudio (R Core Team 2025). Initially, the number of available images, their annual and monthly distribution, and their availability across each 10-year period were evaluated. In this study, each “decade” corresponds to a 10-year period spanning from May of the first year to May of the final year. This approach ensures that each period contains a complete winter season and avoids splitting snow years across two different decades. Subsequently, the temporal evolution of snow cover was examined by producing graphical representations of 500 cloud-free observations, along with the corresponding annual mean and median values. To derive a more robust estimate of the long-term trend in snow cover loss, the mean annual absolute deviation was computed and added to the median. This provides a more statistically reliable measure that accounts for substantial interannual variability in both the number and timing of observations. Using only the mean or median can be misleading in years with limited observations, for example, in 2003, out of the 8 available images, 4 were taken in mid-summer when snow cover was minimal. Finally, a linear regression was calculated on the median plus the mean absolute deviations to provide an approximation of the long-term trend in snow cover for the study area. In cases where two central values occurred (*i.e.*, a tie between medians), their arithmetic mean was used to represent the median for that year.

2.6.2. Snow Persistence

Snow Persistence (SP) represents the fraction of time that snow remains present on the ground (Hammond *et al.* 2018). This metric has been widely applied across different continents and climatic regions to identify snow-covered areas and to compare SP patterns between regions. To calculate SP for each pixel, the formula described by Hammond *et al.* (2018) was used:

$$SP = \frac{\sum S}{(n-ND)} * 100 \qquad \text{(Equation 1)}$$

where S represents the number of observations classified as snow (value 1 in the binary mask), and (n - ND) is the total number of valid observations, with n being the total number of images and ND the number of images discarded due to excessive cloud cover.

To create the SP maps, specific thresholds were established to classify the different areas with similar snow patterns, based on Moore *et al.* (2015). Zones with permanent snow (PSZ), with an SP between 75 % and 100 %, are those where snow persists for most of the year. Zones with seasonal snow (SSZ), with an SP between 50 % and 75 %, are those where snow is present from the beginning to the end of the winter period. Zones with intermittent snow (ItSZ), with an SP between 25 % and 50 %, are those that may remain snow-covered for many days of the year, but the snow cover does not last throughout the winter and undergoes multiple melt events. Zones with infrequent or no snow (InSZ), with an SP between 0 % and 25 %, are areas where snow is almost absent or does not fall every winter. Once the snow classes were defined, SP maps were created for the entire period, from 1984 to 2024.

2.6.3. Snow Line

To estimate the snow line, the SP of each area was combined with NASA's Digital Elevation Model (NASADEM) at 30 m resolution. Snow-covered areas are highly discontinuous and vary considerably due to altitude, aspect, land cover, slope, and, especially, solar irradiance. These factors make it difficult to define a single precise elevation-based snow line. Consequently, in this study, a zonal approach was adopted, similar to that described by Moore *et al.* (2015), in which different elevation bands were classified according to the working scale. First, all the snow and non-snow pixels, along with their height information, were transferred to a vector point file. Then, the average SP was calculated for each 10 m elevation band using RStudio (R Core Team, 2025). This produced a graph showing the variation in SP with elevation for the first and last decade, 1984-1994 and 2014-2024.

2.6.4. Changes in SP and solar irradiance analysis

Once the differences between decades were generated, they were combined with the average solar irradiance maps of the National Park. Solar irradiance was calculated using the hybrid physical, empirical solar irradiance model InsolMets, developed by the GRUMETS research group (Pons & Ninyerola 2008, Roca-Fernández *et al.* 2025). Solar irradiance is a highly valuable geophysical variable, as it not only accounts for orientation and slope, but also integrates cloud optical thickness, cloud fractional cover, the diffuse radiation component and enhanced illumination geometry.

Monthly solar irradiance data (10 kJ/(m²·day)) were grouped over the entire study period. Although a slight increase in solar irradiance was observed over the years, a monthly average was applied to obtain a temporally constant radiation value for each cell throughout the series, while still varying according to geographical location. The full range of values was then divided into eight classes. The use of eight classes of solar irradiance is somewhat reminiscent of a classification into eight directions of topographic orientation. However, solar irradiance is more related to SP since topographic orientation does not differentiate between areas with different degrees of slope, while solar irradiance calculated by InsolMets integrates both variables, in addition to the phenomenon of cast shadowing. These solar irradiance groups, ordered from lowest to highest, were compared with the changes in SP observed by each pixel between the first and last decades (1984-1994 and 2014-2024) and the SP for the entire period (1984-2024). As with solar irradiance, the height of the park was divided into eight equal-sized classes, enabling violin plots to be used to show how height affects SP and the changes in SP between the first and last decades.

Additionally, four linear regression analyses were conducted using a total of 151 124 pixels, considering SP and its decadal changes as dependent variables, and elevation and solar irradiance as independent predictors. A multiple regression analysis was also performed to evaluate the combined influence of both topographic and radiative drivers on SP and recent changes.

3. Results

3.1. Database description

Out of the 903 scenes analysed, 500 were used to calculate SP in the western Catalan Pyrenees, representing 55 % of the total (Figure 2). Only 4 images were available from Landsat-4. For Landsat-5, 272 images were available from 1984 to 2011. In the case of Landsat-7, only 45 images from 1999 to 2003 were used, as the 31 May 2003 Scan Line Corrector (SLC) failure rendered subsequent images unsuitable in the study area. Landsat-8, launched in February 2013, contributed 149 images. The TM sensor on Landsat-5 stopped working over the study area in November 2011, which explains the lack of data for 2012. From autumn 2021 onward, the number of scenes doubled with the launch of the latest Landsat satellite, Landsat-9, which provided 30 images and, together with Landsat-8, continued to acquire data until the present.

The months with the highest number of scenes were the summer months, particularly August, followed by July and September (Figure A.2). Winter was the other season with a high number of scenes, especially December, January, and February. The season with the fewest available scenes was spring, particularly in May, due to cloud cover (Figure A.2). There was a high variability in the number of available scenes due to cloud presence, overlapping acquisition periods between satellites, or the absence of operational satellites. This resulted in an uneven distribution of scenes per year and decade. Decadal groupings (from May of the first year to May of the last year, as previously described) were used to assess long-term changes in SP. The second (1994-2004, 139 images) and last (2014-2024, 169 images) decades had significantly more available scenes than the first (1984-1994, 109 images) and third (2004-2014, 83 images) (Figure 2).

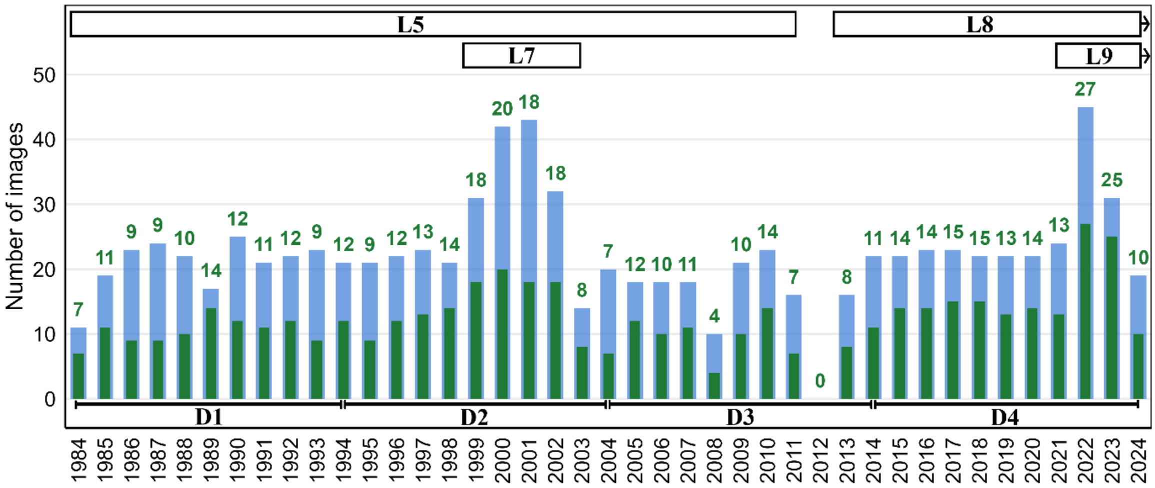

Figure 2. All downloaded images (n=903; blue bars) and all used images (n=500; green bars and green numbers) for the entire study period (1984-2024). Decade 1 (D1): 1984-1994, decade 2 (D2): 1994-2004, Decade 3 (D3): 2004-2014, Decade 4 (D4):2014-2024
Source: own elaboration

3.2. Temporal variability in snow cover

In the western Catalan Pyrenees, a trend towards snow surface loss was observed over the past 40 years (Figure 3). The results accounting for all the observations (Figure 3A) show that the snow surface decreases over time, with a decrease in the number of points near the maximum snow-covered area and an increased density of points below or near 2000 km² in the last decade. The average, median, and the median plus the mean absolute deviation (MAD) of annual snow cover are shown in Figure 3B. A weak negative trend is observed in the linear regression of median + MAD ($Y = -15.36 \times X + 32\,402.96$); the trend is statistically significant with p-value < 0.1 (p-value= 0.097), and the majority of interannual variability remained unexplained ($R^2 = 0.071$). The lack of significance was associated with the large interannual variability in snow cover, as well as variation in the number of observations per year, which reduced the statistical power to detect a clear linear trend. The estimated slope corresponds to an approximate decrease of 15.36 km² per year, but this should be interpreted cautiously.

The seasonal analysis suggested that December, January and February were the months with the greatest snow cover (Figure A.3). In March and April, there was a slight decrease in the average snow-covered surface. June and October corresponded to the last and first snowfall events, respectively, while July, August, and September tended to be free of snowfall events, with no significant accumulations.

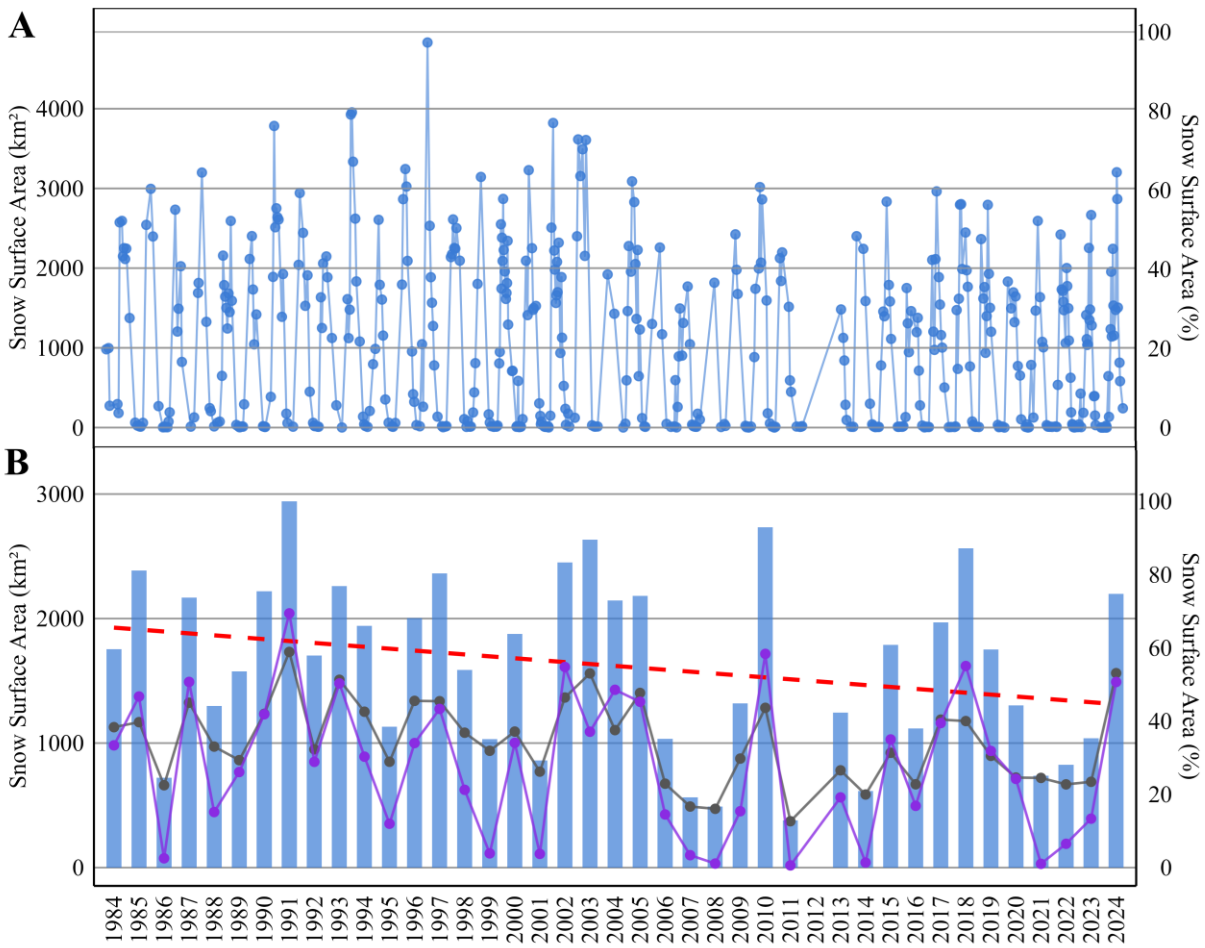

Figure 3. A: Snow cover observations for the entire study period (1984-2024). B: Average annual snow area (grey dots), median annual snow area (purple dots) and the median snow area plus the average of the absolute annual deviations (blue bars) and the regression line with negative slope (red line)

Source: own elaboration

3.3.Spatial variability in SP

In the western Catalan Pyrenees, a large portion of the area belonged to Infrequent Snow Zones (InSZ), accounting for 59 % (2925.26 km^2) of the total surface (Figure 4). This was followed by areas with Intermittent Snow Zones (ItSZ) accounting for 25 % (1229.54 km^2) and those with higher persistence, Seasonal Snow Zones (SSZ), representing 16 % (802.28 km^2), mainly located in the higher elevations near the watershed boundaries that were used to define the study area. Permanent Snow Zones (PSZ) covered only 0.1 % of the total surface (6.14 km^2). These surface values and percentages were calculated without removing projected topographic shadow areas.

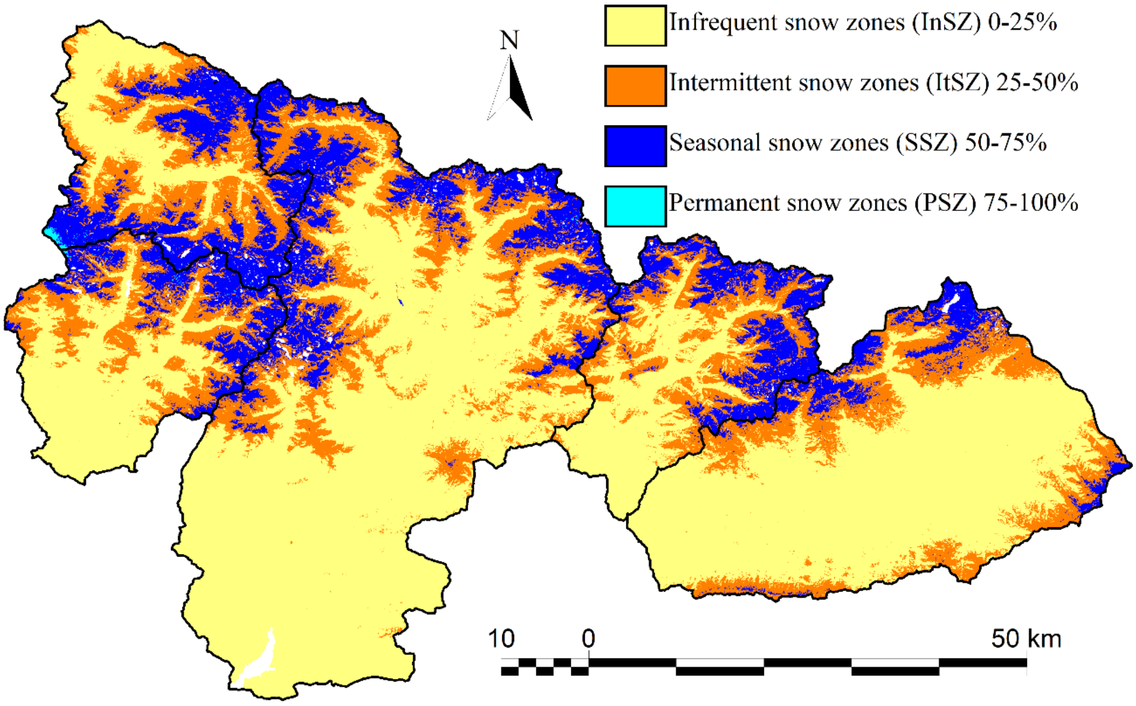

Figure 4. Map of classified SP in the western Catalan Pyrenees from 1984 to 2024. The white areas correspond to water bodies, classified as NoData

Source: Own elaboration. Map obtained from the SP calculation for the entire period and classified into the four SP classes defined in the methodology

3.4. Changes in SP from 1984 to 2024

Over the years, SP in the western Catalan Pyrenees decreased, with 73 % of the area showing a decline and 16 % showing an increase, while 11 % of the surface remained unchanged between the first decade (1984-1994) and the last decade (2014-2024) (Figure 5). Surface and percentage values were calculated with projected topographic shadow areas removed from the analyses. Although the area showing a decrease in SP is much larger than the areas that have remained stable or increased, the pixel-level decrease in SP is often not enough to change the SP class defined in Section 2.6.2 (Figure 5B). Figure A.4 in the appendix shows how the pixels that decreased in SP are represented, in area (km^2) and percentage (%), at the 25th percentile, SP decreased by 11 %, accounting for 81 % of the total affected area.

Most of the surface area has remained in the InSZ class, 2611 km^2 (64.4 %), but if we analyse the pixels that have decreased enough to change the SP class, we find that: 221 km^2 (5.5 %) have gone from ItSZ to InSZ and 261 km^2 (6.4 %) have gone from SSZ to InSZ (Figure5C). Figure A.5 in the appendix shows the differences between SP classes, with the SP maps of the first decade (1984-1994) and the last decade (2014-2024), where it can be clearly observed how the classes of SP that have remained on the surface are the SSZ and the ItSZ.

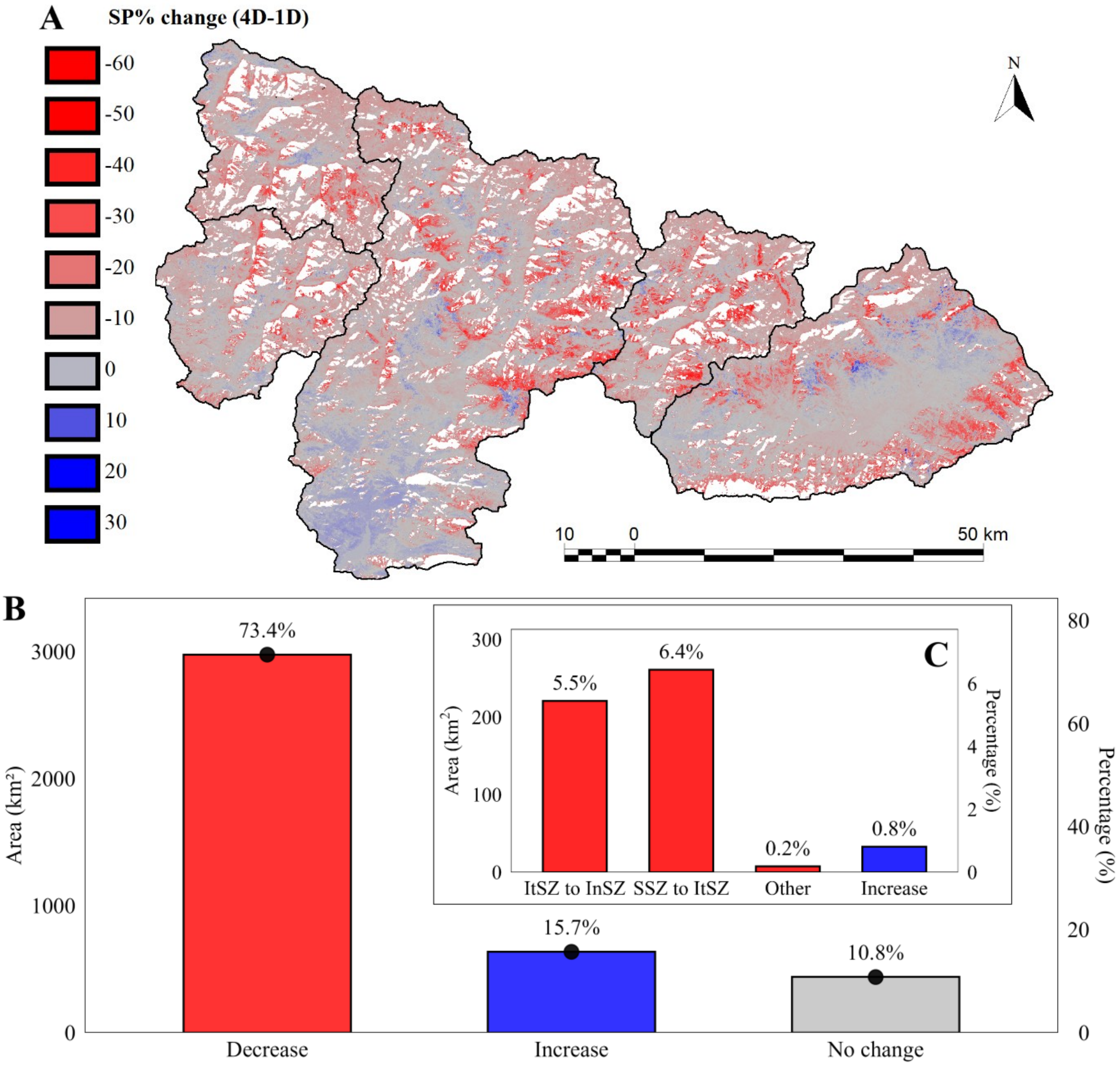

Figure 5. A: Map of changes in SP % in the western Catalan Pyrenees between the first decade, 1D (1984-1993) and the last, 4D (2014-2024). B: Proportion of changes in the western Catalan Pyrenees between 4D and 1D. C: Direction of change. White areas correspond to removed shaded areas classified as NoData
Source: Own elaboration

3.5. Spatiotemporal variability in the snow line

The results in Figure 6 showed differences between the first decade (1984-1994) and last decade (2014-2024). In the lower zones (from 700 m to 1500 m), no major differences were observed between decades due to low persistence of the snow cover; however, from 1500 m upwards, an increase in differences between decades was detected. From 1500 m to 2300 m, SP increases considerably with altitude, but from 2300 to 3000 m, the increase in SP stabilized and the effect of the increase in altitude is not so noticeable. Above 3000 m, SP patterns became more irregular, and a decrease in persistence was observed above 3200 m across both decades.

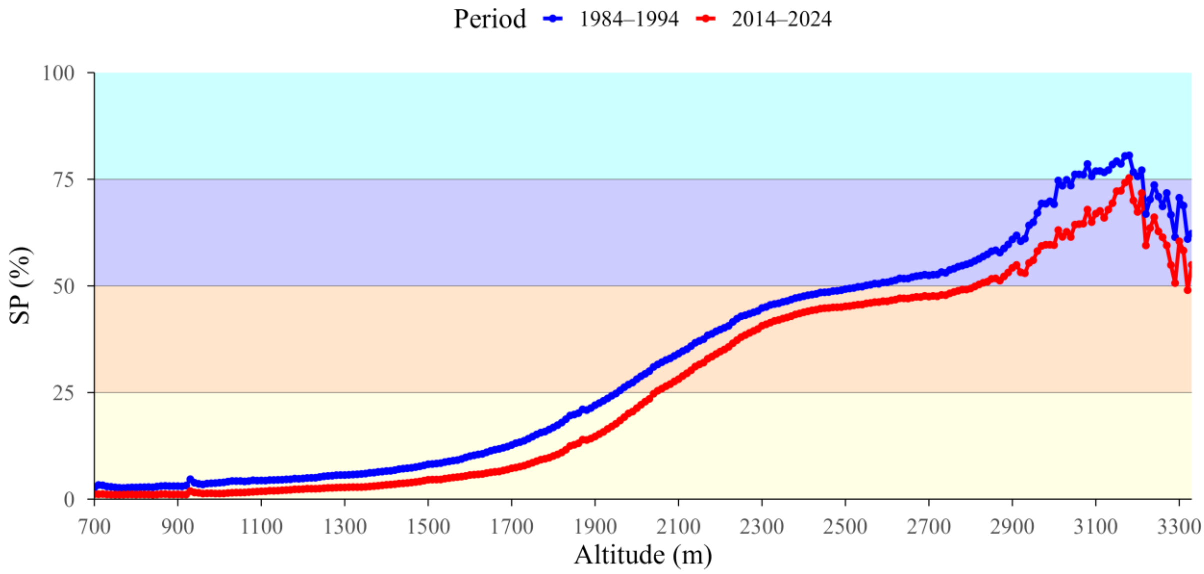

Figure 6. SP (%) and altitude (m) for decades 1D (1984-1994) and 4D (2014-2024) snow line
Source: own elaboration

Figure 6 also shows the altitude at which the change of SP classes occurs. Considering the snow zones defined in Section 2.6.2, the transition from InSZ to ItSZ (SP = 25 %) in the first decade occurs at an altitude of 1953 m, while in the last decade it occurs at 2044 m. The transition from ItSZ to SSZ (SP = 50 %) is the one showing the greatest altitude difference; it goes from 2546 m in the first decade to 2812 m in the last one. The transition from SSZ to PSZ (SP = 75 %) occurs at 3040 m and 3177 m, respectively, but then, with increasing height, a decrease in SP is observed. The point with highest SP in the first decade is at an altitude of 3180 m with an SP of 80.6 %, and the point with the highest SP in the last decade is also at exactly 3180 m, with a SP of 75.3 %.

3.6. Drivers of SP

Figure 7 shows that SP increases with elevation (Figure 7A) and decreases slightly with increased solar irradiance (Figure 7B) in the Aigüestortes and Estany de Sant Maurici National Park. However, as expected, the group with the highest solar irradiance (1490 - 1580 10 kJ/(m²·day)) corresponds to the lowest SP value. In contrast, when analysing the difference in SP between the fourth (2014-2024) and first (1984-1994) decades (Figure 7C and 7D), a very smooth but similar trend emerged in both cases: the magnitude of the change decreased with increasing elevation and solar irradiance.

To further explore the spatial controls on snow dynamics, we conducted four simple linear regressions using the complete dataset (n = 104 246 pixels). Two of the models used long-term SP (1984-2024) as the dependent variable, and the other two analysed the difference in SP between the fourth and first decades (4D-1D). In each case, elevation and solar irradiance were tested separately as predictors. All linear regression analyses are statistically significant.

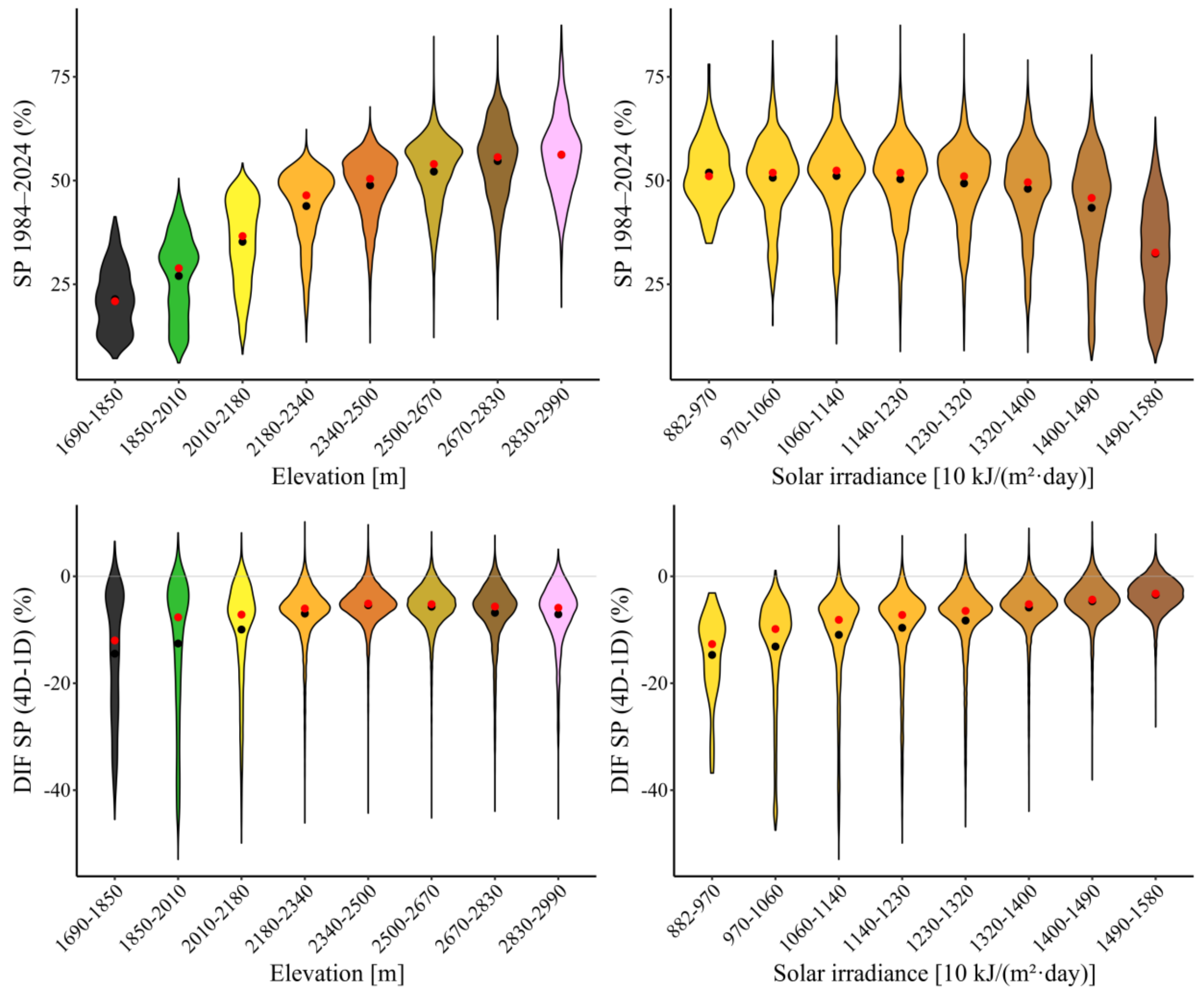

Figure 7. Violin plot of SP with height (7A); SP with solar irradiance (7B); Changes in SP and altitude (7C); changes in SP and solar irradiance (7D) in the Aigüestortes and Estany de Sant Maurici National Park. The black dots indicate the mean and the red dots the median of SP and SP differences between decades

Source: Own elaboration

Model	Dependent Variable (Y)	Predictor Variable (X)	Formula	R^2	*p*-value
A	SP 1984-2024	Elevation	Y = -29.09 + 0.030X	0.361	< 0.0001
B	SP 1984-2024	Solar irradiance	Y = 89.01 - 0.034X	0.121	< 0.0001
C	DIF (4D-1D)	Elevation	Y = -16.3 + 0.004X	0.026	< 0.0001
D	DIF (4D-1D)	Solar irradiance	Y = -37.2 + 0.024X	0.195	< 0.0001

Table 1. Linear regression analysis table. Regression between SP for the entire study period (SP 1984-2024) and Elevation (A) and Solar irradiance (B). Regression between changes in SP between 4D (2014-2024) and 1D (1984-1994) with Elevation (C) and Solar irradiance (D).

Source: own elaboration.

The results showed that elevation explained a significant portion of the variability in SP ($R^2 = 0.361$), with higher elevations being associated with greater persistence values. The slope of the regression (0.03) indicated a consistent positive relationship. In contrast, solar irradiance presented a weaker negative relationship ($R^2 = 0.121$), and a negative slope (-0.034) confirmed that areas with greater exposure tended to show lower SP, in line with physical expectations. Regarding changes in SP between decades, DIF (4D-1D), both results showed very low explanatory power, solar irradiance had slightly higher explanatory power ($R^2 = 0.195$) compared to elevation ($R^2 = 0.026$), suggesting that solar irradiance played a more important role in modulating the intensity of decadal changes.

Below is a brief interpretation of the results of the two multiple regression models with respect to altitude and solar irradiance. Model 1: SP. Model 2: change in SP between decades.

Model 1, SP (1984–2024): This multiple regression model explains the variability of SP over the entire study period (1984–2024) based on altitude and solar irradiance. The correlation coefficient of 0.688 indicates a clear relationship between the predictors and SP. The model explains 47.4 % of the variance in SP and is statistically significant ($p < 0.0001$). For each additional meter of height, SP increases by 0.03 units, keeping radiation constant, and for each extra unit of radiation, persistence decreases by 0.03 units, keeping height constant. The mean error less than 10 % suggests that the model does not exhibit systematic bias.

Model	Dep. Variable	Predictors	Corr.	R^2	RMS	Alt. Coef.	S.Rad Coef.	*p*-value
1	SP 1984-2024	Altitude + Solar.Rad	0.688	0.474	8.740	+0.0296	−0.0331	< 0.0001
2	Diff_4D_1D		0.474	0.224	5.815	+0.0047	+0.0241	< 0.0001

Table 2. Main results of the two multiple regressions.
RMS values are expressed as percentages (%), the same units as SP.
Source: own elaboration based on multiple regression analysis

Model 2, Difference in SP between decades (2014–2024 and 1984–1994): This model assesses the change in SP between the fourth and first decades as a function of altitude and solar irradiance. The correlation (0.474) is slightly lower than in the first model, with the model explaining 22.4 % of the variance in this difference. Both altitude and solar irradiance have positive coefficients: for each additional meter of height, the SP difference increases by 0.005 units. Unlike the first model, here higher solar radiation increased the SP difference; for each extra unit of radiation, the SP difference increased by 0.02. This model is also highly significant ($p < 0.0001$).

4. Discussion

4.1. Database consistency and snow cover classification challenges

Around 903 Landsat scenes were analysed, but only slightly more than half were used to calculate SP. Temporal cloud gaps in the series, differences in atmospheric correction algorithms between platforms, variability in temporal resolution, as well as satellite discontinuity and overlap, affected the temporal representativeness of the data. Seasonal variation in scene availability was also evident, with peaks in data acquisition during summer and winter, and very limited coverage in spring, particularly in May. Nevertheless, SP monitoring was made possible thanks to the high number of available images. Although the SP estimates were insufficient for more detailed temporal analyses (*e.g.*, assessing seasonal variability or detecting changes in the timing and duration of snowfall and snow cover during the thaw season), they were adequate for determining the proportion of time snow remained on the ground each decade.

Regarding snow classification, this study found that the commonly used NDSI threshold of 0.4 was sufficient. Using lower values improved the detection of hidden snow but also increased commission errors, particularly confusion with clouds or water bodies. We verified that changes in the threshold value did not substantially alter the detected snow-covered area. Important issues were also detected when using Landsat Collection 2, Level 2 images: the checkerboard effect in the NDSI for Landsat-5 and Landsat-7, and the presence of pixels classified as NoData in shadowed areas for Landsat-8 and Landsat-9, made comparisons between images and decades difficult (*see Section 4.5 and Figures A9 and A10*).

Another challenge was the misclassification of water bodies as snow, especially when they were partially frozen. The changing physical state of water depending on climatic conditions (snow, ice, liquid water) complicates accurate detection in areas with large elevation gradients, such as the study area, where different water states could coexist within a single image. To address this, a water mask was applied to remove all water bodies from the calculations. However, this approach also excluded snow persisting on frozen lake surfaces during winter, which could affect the quantity and chemical composition of water available in the basin. This aspect should be considered in greater detail in future studies.

4.2. Patterns and drivers of snow persistency

The results in Figure 3A revealed a clear downward trend in snow cover across the entire study area, likely related to climate change, such as rising temperatures or changes in precipitation patterns. The regression line in Figure 3B was calculated using the sum of median and mean absolute deviation (MAD) to homogenize sample numbers and account for years with few dates. This indicates an annual loss of 15.36 km² in the study area, and it is consistent with other studies showing snow cover loss above 2100 m (López-Moreno *et al.* 2020).

Changes in snow surface reflect the Mediterranean climate influence over the southern and eastern Pyrenees, characterized by high interannual variability (Barrou Dumont *et al.* 2024). Snow cover reached its maximum in December–February, decreased markedly in March–April, and almost disappeared in July, illustrating the strong seasonality of the snowpack (Figure A.4).

Overall, there was a shift towards a more intermittent regime, with increases in areas of infrequent SP and decreases in permanent or seasonal SP (Figure 5.B). Regions where snow previously persisted all winter now melted more rapidly and lasted less time on the ground. Permanent snow areas became almost residual, highlighting high mountain zones as refuges for snow. Figure A.5 shows the low representation of permanent snow zones on the map of the classified SP in the western Catalan Pyrenees.

It is important to note that although most surfaces have experienced a decrease in SP (Figure 5B), 73 % of all areas without shadows that decreased in SP lost only between 1 % and 11 % (Figure A.4). This loss of SP may not be sufficient to change their persistence class. Areas with intermittent or seasonal persistence were the most susceptible to change (Figure 5C). Only 11 % of the surface remained completely unchanged in SP class between the 1984-1994 and 2014-2024 decades, but most pixels have not shifted class despite evidence of persistence loss. Meanwhile, 16 % of the area showed an increase in SP, mainly in areas of sparse vegetation and alpine meadows, likely due to wind redistribution. An increase in snow persistence is also observed in anthropized areas, such as ski resorts, where snow is produced by cannons and compacted by snow groomers (*see Figure A.8 in the appendix*).

4.3. Changing snow lines

The altitudinal analysis showed a decrease in SP with height between the first and last decades, averaging 4.8 %. The maximum difference, 7.1 %, occurred in the seasonal snow zone (SP = 50-75 %) at 3 270 m, in the highest and most rugged areas where strong winds and topography limit snow persistence. Differences of 5.0 % and 3.3 % were observed in the intermittent (SP = 25-50 %) and infrequent (SP = 0-25 %) zones, respectively. The seasonal snow line (SP = 50 %) rose from 2 546 m in the first decade to 2 813 m in the last, an increase of 267 m.

According to these results, the areas that have experienced the greatest change in SP between the first and last decades were the higher parts of the study area and those with seasonal snow cover. These findings are consistent with Hammond *et al.* (2018), who identified the strongest interannual variability in SP at mid elevations, near the boundary between intermittent and seasonal snow zones.

4.4. Changes in SP in relation to altitude and solar irradiance in the park.

The results of section 3.6 show that areas receiving more solar irradiance experienced relatively minor SP changes between decades, whereas low-radiation zones showed more pronounced reductions. As shown in Figures A6 and A7 in the appendix, maps of SP and solar irradiance (10 kJ/(m²·day)) from 2004 to 2020 indicate that areas with higher SP do not always correspond to zones with lower solar radiation. In the lower, often enclosed areas of the park, SP was lower than in more exposed, higher-altitude zones, despite receiving less solar irradiance. This may explain why the violin plots and linear regressions did not show a clear decrease in SP with increasing solar irradiance: many low-lying areas had both low SP and low irradiance.

The linear regression between SP for the period 1984-2024 and elevation (Table 1) shows a slope of 0.03, meaning that SP increases by 3 % every 100 m. In contrast, the relationship between SP and solar irradiance shows a negative slope (−0.0344): for every 10 kJ/(m²·day) increase, SP decreases by 3.4 %. Model A explains 36.1 % of the variance for altitude, whereas Model B explains 12.1 % for solar irradiance. This suggests that persistence depends heavily on altitude: the higher the altitude, the greater the SP. Although solar irradiance is weaker predictor of SP, all the models are statistically significant (p-value < 0.0001). Considering that altitude is already included in solar radiation calculations, other climatic and geomorphological factors likely influenced SP more than solar irradiance. These findings are consistent with the eight-group classification (Figure 6), which showed that the decrease of SP with increasing irradiance was not uniform: the highest-irradiance group had the lowest average SP, but the park-wide pattern was not uniformly decreasing. When considering decadal SP changes (DIF 4D-1D, Table 1), neither variable explained much variability; however, irradiance showed slightly greater explanatory power (19.5 %) than altitude (2.6 %).

Areas with greater solar irradiance and altitude experienced smaller SP changes between 1984–1994 and 2014–2024 (Figure 7). In the case of altitude, this is likely because higher elevations are associated with lower temperatures, allowing snow to remain longer and reducing the magnitude of recent changes. Regarding solar irradiance, many highly exposed areas, such as south-facing slopes or zones with little accumulation, already had low SP at the beginning of the study period. This left little room for further decline, and the effect of recent climate change was less pronounced in these locations.

When elevation and radiation were considered together, the models captured more overall variability, highlighting how these factors interact to shape snow-cover behaviour (Table 2). A comparison of the two multiple regression models revealed that changes in SP between decades are less strongly correlated with, and less explained by, altitude and solar irradiance than long-term SP. This suggests that other factors influenced the reduction in SP between 1984-1994 and 2014-2024. Some of the remaining unexplained variability was likely due to factors not included in these models, such as wind, humidity, vegetation and land cover (including canopy density), and human activities, in addition to temperature and precipitation.

4.5. Challenges in snow cover detection and temporal analysis. Some recommendations for future work.

Despite the overall robustness of the methodology used, several limitations have been identified that should be addressed in future studies to enhance the reliability and applicability of the results. These data are an approximation, and the low number of images in some years may introduce bias into the results. The low temporal resolution of the Landsat archive, combined with extended data gaps sometimes exceeding 30 days, hindered the analysis of seasonal and phenological patterns. We propose complementing the dataset with other freely available multispectral platforms, such as Sentinel-2 or MODIS, to improve temporal and spatial resolution and obtain more precise estimates of SP, including the timing of snowfall and melt periods.

Another critical aspect concerns snow detection in projected topographic shadow areas. Was observed that differences in radiometric correction algorithms between sensors (LEDAPS vs. LaSRC) can lead to substantial inconsistencies in snow detection within these zones.

As mentioned above, the Landsat-5 image from December 20, 1990 (Figure A.9) showed a snow classification with excessive commission errors, where pixels in shadows are classified as snow with low certainty. This image, in the southwest of the National Park, shows a distinct 'checkerboard' pattern, which is associated with extremely low radiometric signal values. This pattern was repeated in most Landsat-5 and Landsat-7 winter images, when solar elevation is minimal. The checkerboard pattern and commission errors were even more pronounced in areas further south and at lower elevations, where no snow was present but the NDSI still classified pixels as snow.

Under these conditions, incident solar irradiance is insufficient to obtain enough spectral response in both the green and SWIR bands. When calculating the normalized difference snow index (NDSI = (ρV − ρSWIR) / (ρV + ρSWIR)), the presence of very low and similar values in both bands means that the denominator of the expression is very small. In this scenario, small absolute variations in reflectance, derived from radiometric noise, the sensor quantization, or minimal differences in illumination, result in large relative variations in the quotient. Consequently, the NDSI can reach artificially high values in the absence of real snow, generating systematic false positives in shaded areas (Figure A.9). This numerical instability is inherent in normalized indices when the denominator approaches zero, causing pixels with very similar physical spectral responses to have contrasting index values. For this reason, the exclusive use of the NDSI and the choice of threshold represent a methodological limitation, as this parameter is subjective and may introduce variability in the results. In this sense, the use of supervised classification methods, such as the k-NN classifier, is proposed for future research. These approaches can integrate multiple spectral bands and indices (*e.g.*, NDSI, NDWI) and define specific training areas to improve the discrimination between snow, water, and clouds.

As another example of snow classification in Landsat-8 and Landsat-9 images, such as Figure A.10 from December 22, 2014. As mentioned, the LaSRC radiometric correction algorithms did not correct most pixels in projected topographic shadows. This is a known issue reported by the USGS: “Landsat-8 and Landsat-9 C2 Surface Reflectance products may contain 'NoData' pixels on the edges of clouds even though the QA band does not indicate a NoData pixel. This artifact is more frequent at the shorter wavelengths and usually occurs over dark water pixels and shadowed land pixels under low solar illumination conditions”.

The combination of both limitations, the checkerboard pattern in NDSI from Landsat-5 and Landsat-7 (LEDAPS) and the presence of NoData pixels in shadows from Landsat-8 and Landsat-9 (LaSRC), make it difficult to compare snow cover across dates from different platforms, especially in winter scenes, unless these areas are avoided, as in this study. A clear example is the comparison of NDSI-based snow cover on December 20, 1990, and December 22, 2014 (Figures A9 and A10, in the appendix). Reliable comparisons of snow cover for similar dates across years and platforms are nearly impossible due to the differences in shaded areas, with pixels containing data versus 'NoData', between dates. Despite these technical challenges, we recommend using uncorrected Level 1 images and applying a consistent, custom atmospheric correction to all scenes to build a more homogeneous dataset.

5. Conclusions

The results of this study show a clear and sustained decrease in SP in the western Catalan Pyrenees, with potentially significant implications for the hydrology, ecology and biogeochemistry of high mountain catchments. This pattern reflects a widespread transition from seasonal snow to a more intermittent regime, along with an almost complete disappearance of areas with permanent snow.

The spatial analysis of SP confirms that most areas with reduced persistence correspond to transitions from seasonal to intermittent snow 261 km^2 (6.4 %), or transitions from intermittent to infrequent snow zones 221 km^2 (5.5 %). These changes are likely to affect the land surface energy budget and to influence hydrological responses and ecosystem functioning.

Analysis of the snow line elevation indicates a significant decrease in SP during the most recent decade (2014–2024) compared to the first decade of the study period (1984–1994). While this decrease is consistent with the effects of ongoing climate warming, part of the observed signal may also be influenced by methodological limitations related to differences in radiometric correction and snow detection in shaded areas. Therefore, these results should be interpreted with caution, as this study represents a preliminary assessment based on a single remote-sensing platform group with limited temporal resolution and a simplified snow classification approach.

The multiple regression models indicate that elevation remains a key driver of the long-term spatial distribution of SP. Although solar irradiance has a weaker influence on spatial patterns, it appears to play a more pronounced role in modulating temporal changes in SP. Combining elevation and solar irradiance as predictors improves model performance and provides a more robust framework for understanding SP dynamics.

Snow persistence at mid-elevations appears to be particularly sensitive to ongoing climate change, whereas higher-elevation areas show more stable behaviour. This suggests that additional climatic and environmental factors not included in the current models contribute to the observed variability in SP, particularly temperature and precipitation. Future work should therefore integrate key climate variables to better characterise long-term trends in snow persistence.

Finally, this study highlights the need for multi-sensor approaches and advanced classification methods to better capture snow persistence dynamics in complex mountainous terrain. Based on the current results, no clear decrease in snowfall can be concluded, but significant changes in snow persistence have been detected. As discussed throughout this study, future analyses of SP will require higher temporal resolution.

Overall, this work provides a solid foundation for further research into snowpack dynamics in the western Catalan Pyrenees and their environmental implications, while also highlighting opportunities to improve snow monitoring methodologies using remote sensing.

6. Acknowledgments

This work was supported by the CSIC Special Intramural Project (PIE) BIOGEOMONT ("Alterations in the Biogeochemical Cycles of High-Mountain Watersheds in the Context of Global Change: Implementation of a Monitoring Plan", project code 20243MAX010), funded through the RYC-MaX 2023 Excellence Grant by the Spanish Ministry of Science, Innovation and Universities (MICIU), the Spanish State Research Agency (AEI, Grant 10.13039/501100011033), and the European Social Fund Plus (ESF+).

This work was carried out within the framework of the PhD Programme in Geography at the Universitat Autònoma de Barcelona. I would also like to thank the Department of Geography at the Universitat Autònoma de Barcelona, the Methods and Applications in Remote Sensing and Geographic Information Systems Research Group (GRUMETS), and the Institute of Environmental Assessment and Water Research (IDAEA-CSIC) for their scientific and institutional support. Finally, I am especially grateful to my PhD supervisors, Lluís Gómez Gener and Xavier Pons, and to Lluís Pesquer and Cristina Cea for their guidance, encouragement, and continued support throughout my doctoral research.

References

Anenberg, A. N. (2019). *Effects of snow persistence on soil water nitrogen across an elevation gradient* [Colorado State University]. https://hdl.handle.net/10217/199784

Barrou Dumont, Z., Gascoin, S., Inglada, J., Dietz, A., Köhler, J., Lafaysse, M., Monteiro, D., Carmagnola, C., Bayle, A., Dedieu, J.-P., Hagolle, O., & Choler, P. (2024). *Trends in the annual snow melt-out day over the French Alps and the Pyrenees from 38 years of high resolution satellite data (1986–2023)*. Snow/Seasonal Snow. https://doi.org/10.5194/egusphere-2024-3505

Brooks, P. D., & Williams, M. W. (1999). Snowpack controls on nitrogen cycling and export in seasonally snow-covered catchments. *Hydrological Processes*, *13*(14–15), 2177–2190. https://doi.org/10.1002/(SICI)1099-1085(199910)13:14/15%253C2177::AID-HYP850%253E3.0.CO;2-V

Cea, Cristina., Cristóbal Rosselló, J., & Pons, X. (2007). *Determinación de la superficie nival del Pirineo catalán mediante imágenes Landsat y MODIS*. XII Congreso Nacional de Tecnologías de la Información Geográfica. https://www.researchgate.net/publication/239926802_Determinacion_de_la_superficie_nival_del_pirineo_catalan_mediante_imagenes_Landsat_y_MODIS

Choi, G., Robinson, D. A., & Kang, S. (2010). Changing Northern Hemisphere Snow Seasons. *Journal of Climate*, *23*(19), 5305–5310. https://doi.org/10.1175/2010JCLI3644.1

Cuadrat, J. M., Serrano-Notivoli, R., Prohom, M., Cunillera, J., Tejedor, E., Saz, M. Á., De Luis, M., Llabrés-Brustenga, A., & Soubeyroux, J.-M. (2024). Climate of the Pyrenees: Extremes indices and long-term trends. *Science of The Total Environment*, *933*, 173052. https://doi.org/10.1016/j.scitotenv.2024.173052

Dozier, J. (1989). Spectral signature of alpine snow cover from the landsat thematic mapper. *Remote Sensing of Environment*, *28*, 9–22. https://doi.org/10.1016/0034-4257(89)90101-6

Dumont, B. (2025). *Reconstruction par imagerie satellite de la couverture neigeuse des Alpes et Pyrénées sur une période couvrant les 37 dernières années*. https://theses.hal.science/tel-05043839v1

Gascoin, S., Barrou Dumont, Z., Deschamps-Berger, C., Marti, F., Salgues, G., López-Moreno, J. I., Revuelto, J., Michon, T., Schattan, P., & Hagolle, O. (2020). Estimating Fractional Snow Cover in Open Terrain from Sentinel-2 Using the Normalized Difference Snow Index. *Remote Sensing*, *12*(18), 2904. https://doi.org/10.3390/rs12182904

Girona-Mata, M., Miles, E. S., Ragettli, S., & Pellicciotti, F. (2019). High-Resolution Snowline Delineation From Landsat Imagery to Infer Snow Cover Controls in a Himalayan Catchment. *Water Resources Research*, *55*(8), 6754–6772. https://doi.org/10.1029/2019WR024935

Hall, D. K., & Riggs, G. A. (2007). Accuracy assessment of the MODIS snow products. *Hydrological Processes*, *21*(12), 1534–1547. https://doi.org/10.1002/hyp.6715

Hammond, J. C., Saavedra, F. A., & Kampf, S. K. (2018). Global snow zone maps and trends in snow persistence 2001–2016. *International Journal of Climatology*, *38*(12), 4369–4383. https://doi.org/10.1002/joc.5674

Härer, S., Bernhardt, M., Siebers, M., & Schulz, K. (2018). On the need for a time- and location-dependent estimation of the NDSI threshold value for reducing existing uncertainties in snow cover maps at different scales. *The Cryosphere*, *12*(5), 1629–1642. https://doi.org/10.5194/tc-12-1629-2018

Hori, M., Sugiura, K., Kobayashi, K., Aoki, T., Tanikawa, T., Kuchiki, K., Niwano, M., & Enomoto, H. (2017). A 38-year (1978–2015) Northern Hemisphere daily snow cover extent product derived using consistent objective criteria from satellite-borne optical sensors. *Remote Sensing of Environment*, *191*, 402–418. https://doi.org/10.1016/j.rse.2017.01.023

López-Moreno, J. I., Soubeyroux, J. M., Gascoin, S., Alonso-Gonzalez, E., Durán-Gómez, N., Lafaysse, M., Vernay, M., Carmagnola, C., & Morin, S. (2020). Long-term trends (1958–2017) in snow cover duration and depth in the Pyrenees. *International Journal of Climatology*, *40*(14), 6122–6136. https://doi.org/10.1002/joc.6571

Moore, C., Kampf, S., Stone, B., & Richer, E. (2015). A GIS-based method for defining snow zones: Application to the western United States. *Geocarto International*, *30*(1), 62–81. https://doi.org/10.1080/10106049.2014.885089

Morán-Tejeda, E., López-Moreno, J. I., & Sanmiguel-Vallelado, A. (2017). Changes in Climate, Snow and Water Resources in the Spanish Pyrenees: Observations and Projections in a Warming Climate. In J. Catalan, J. M. Ninot, & M. M. Aniz (Eds.), *High Mountain Conservation in a Changing World* (Vol. 62, pp. 305–323). Springer International Publishing. https://doi.org/10.1007/978-3-319-55982-7_13

Painter, T. H., Rittger, K., McKenzie, C., Slaughter, P., Davis, R. E., & Dozier, J. (2009). Retrieval of subpixel snow covered area, grain size, and albedo from MODIS. *Remote Sensing of Environment*, *113*(4), 868–879. https://doi.org/10.1016/j.rse.2009.01.001

Pons, X. (2004). *MiraMon. Sistema d'Informació Geogràfica i software de Teledetecció* [Computer software]. Centre de Recerca Ecològica i Aplicacions Forestals, CREAF. https://www.miramon.cat/

Pons, X., Cea, C., González-Guerrero, Ó., & Cristóbal, J. (2025). Landsat Collection 2: Key Information and recommendations for data users and product developers. *Revista de Teledetección*, (66). https://doi.org/10.4995/raet.2025.23510

Pons, X., & Ninyerola, M. (2008). *Mapping a topographic global solar radiation model implemented in a GIS and refined with ground data* [Computer software]. https://rmets.onlinelibrary.wiley.com/doi/10.1002/joc.1676

Robinson, D. A., Estilow, T. W., & NOAA CDR Program. (2015). *NOAA Climate Data Record (CDR) of Northern Hemisphere (NH) Snow Cover Extent (SCE), Version 1* [Dataset]. NOAA National Centers for Environmental Information. https://doi.org/10.7289/V5N014G9

Roca-Fernández, C., Pons, X., & Ninyerola, M. (2025). A Comparison of Different Solar Radiation Models in the Iberian Peninsula. *Atmosphere*, *16*(5), 590. https://doi.org/10.3390/atmos16050590

Salomonson, V. V., & Appel, I. (2004). Estimating fractional snow cover from MODIS using the normalized difference snow index. *Remote Sensing of Environment*, *89*(3), 351–360. https://doi.org/10.1016/j.rse.2003.10.016

Sayler, K. (2021). *Landsat 4-7 Collection 2 (C2) Level 2 Science Product (L2SP) Guide*.

Sayler, K. (2023). *Landsat 8-9 Collection 2 Level 2 Science Product Guide*.

Wipf, S., Sommerkorn, M., Stutter, M. I., Wubs, E. R. J., & Van Der Wal, R. (2015). Snow cover, freeze-thaw, and the retention of nutrients in an oceanic mountain ecosystem. *Ecosphere*, *6*(10), 1–16. https://doi.org/10.1890/ES15-00099.1

Zhang, H., Zhang, F., Zhang, G., Che, T., Yan, W., Ye, M., & Ma, N. (2019). Ground-based evaluation of MODIS snow cover product V6 across China: Implications for the selection of NDSI threshold. *Science of The Total Environment*, *651*, 2712–2726. https://doi.org/10.1016/j.scitotenv.2018.10.128

7. APPENDIX

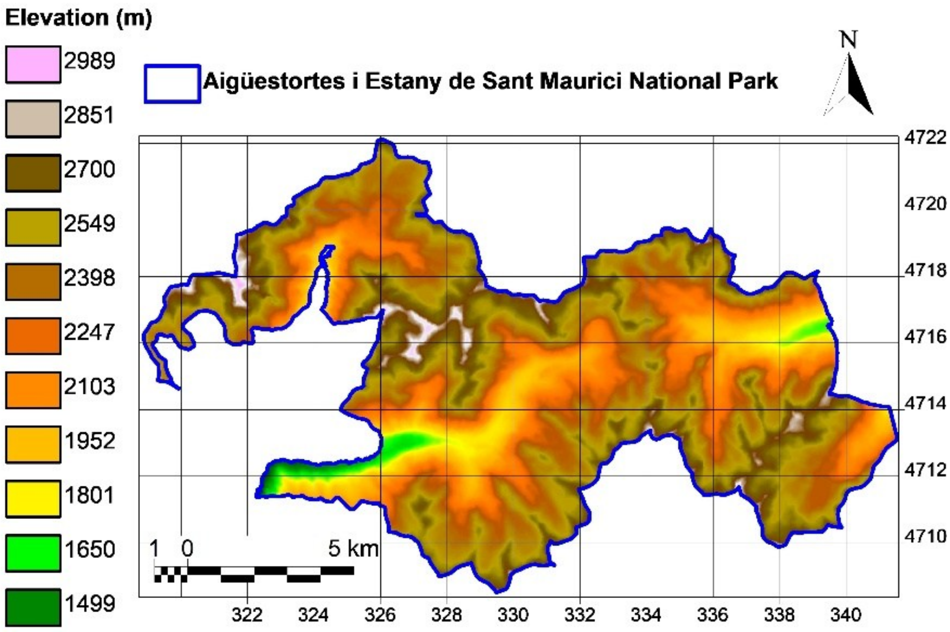

Figure A.1. Elevation map of Aigüestortes i Estany de Sant Maurici National Park. UTM-31N projection; coordinates in km

Source: own elaboration based on the 30 m DEM (NASADEM)

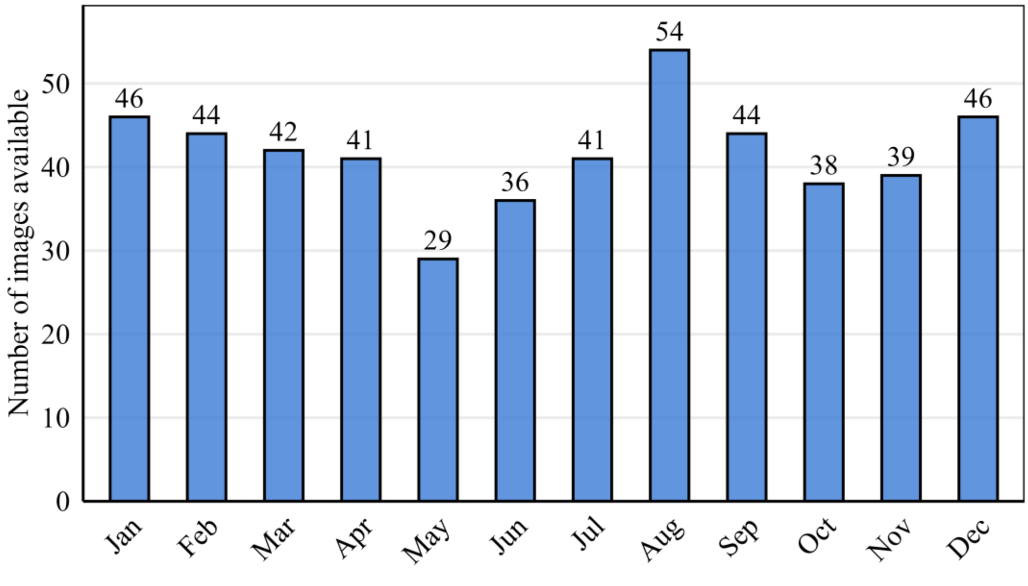

Figure A.2. Number of images available per month for the entire period of study (1984-2024)

Source: Own elaboration

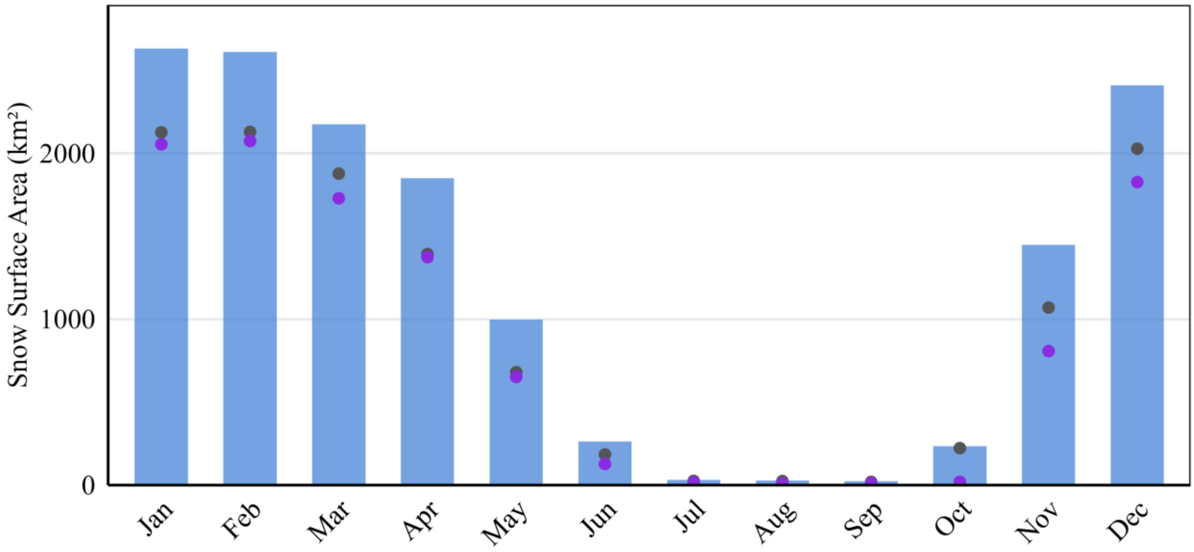

Figure A.3. Average monthly snow area (grey dots), median monthly snow area (purple dots) and the median snow area plus the average of the absolute month deviations (blue bars) Catalan Pyrenees from 1984 to 2024
Source: Own elaboration

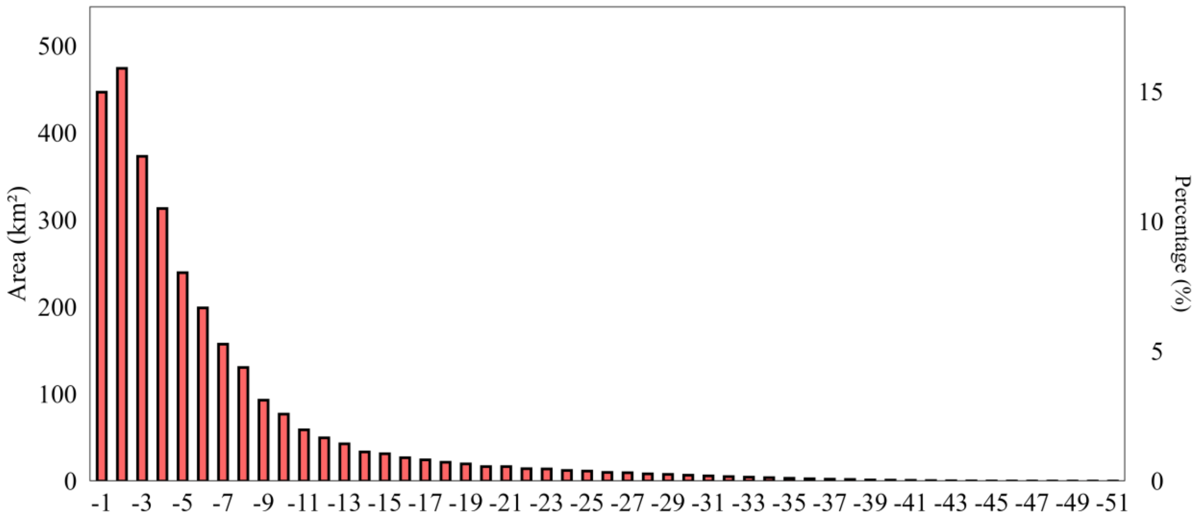

Figure A.4. Distribution of pixels that have decreased in SP between the first (1984-1994) and last decade (2014-2024)
Source: Own elaboration

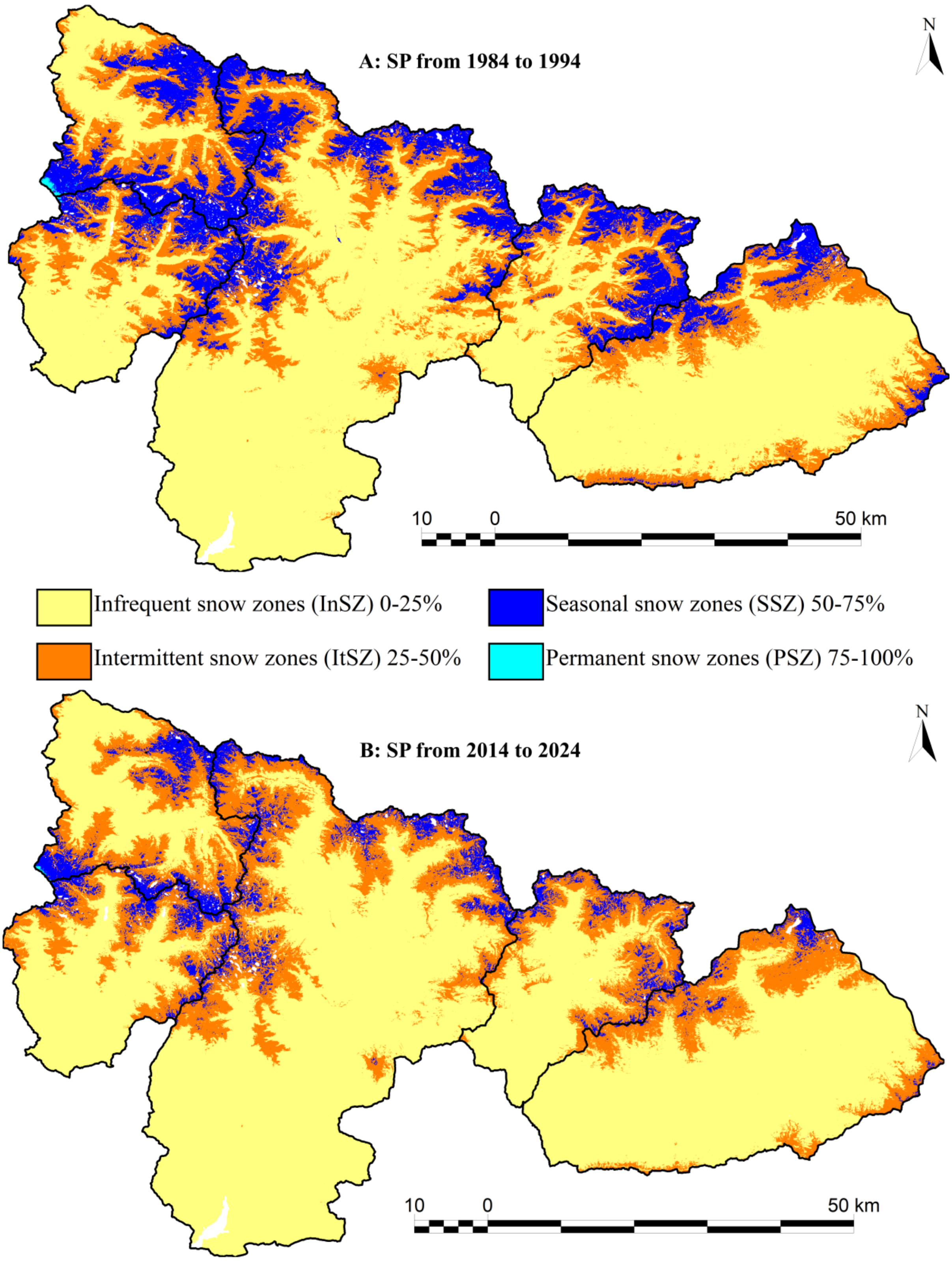

Figure A.5. Map of classified SP in the western Catalan Pyrenees. A: SP from 1984 to 1994. B: SP from 2014 to 2024. The white areas correspond to water bodies, classified as NoData

Source: Own elaboration. Map resulting from the calculation of the SP for the entire period with the equation of section 3.4.1 and classified with the 4 classes of SP defined in section 3.5.2

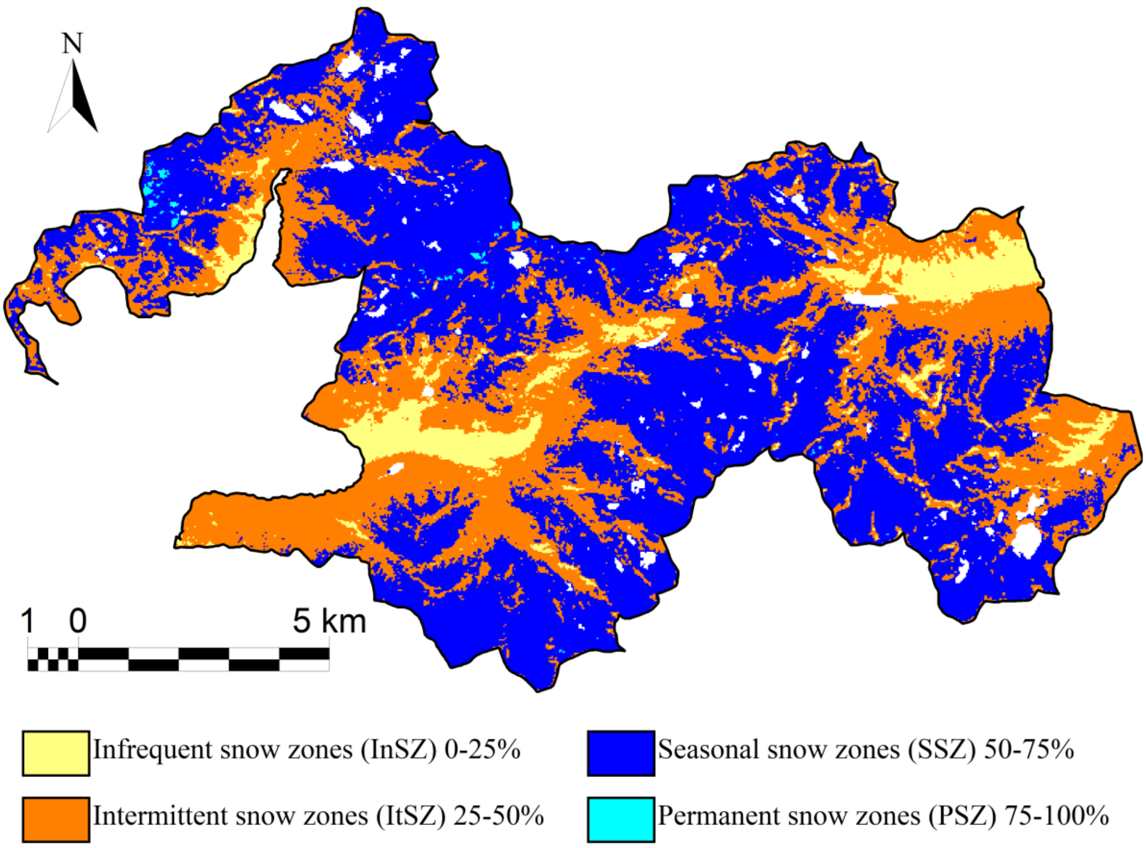

Figure A.6. Map of classified SP in the Aigüestortes i Estany de Sant Maurici National Park from 1984 to 2024. The white areas correspond to water bodies, classified as NoData

Source: Own elaboration. Map resulting from the calculation of the SP for the entire period with the equation of section 3.4.1 and classified with the 4 classes of persistence defined in section 3.5.2

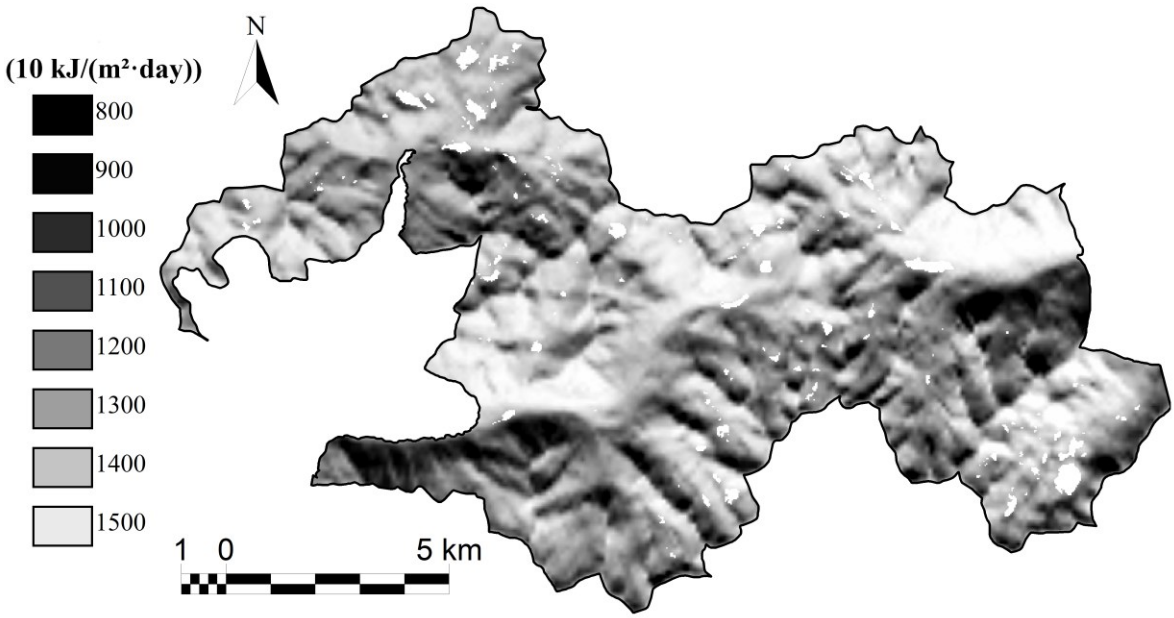

Figure A.7. Monthly solar irradiance in the Aigüestortes National Park National Parc (10 kJ/(m²·day)). The white areas correspond to water bodies, classified as NoData

Source: Roca-Fernández *et al.* (2025)

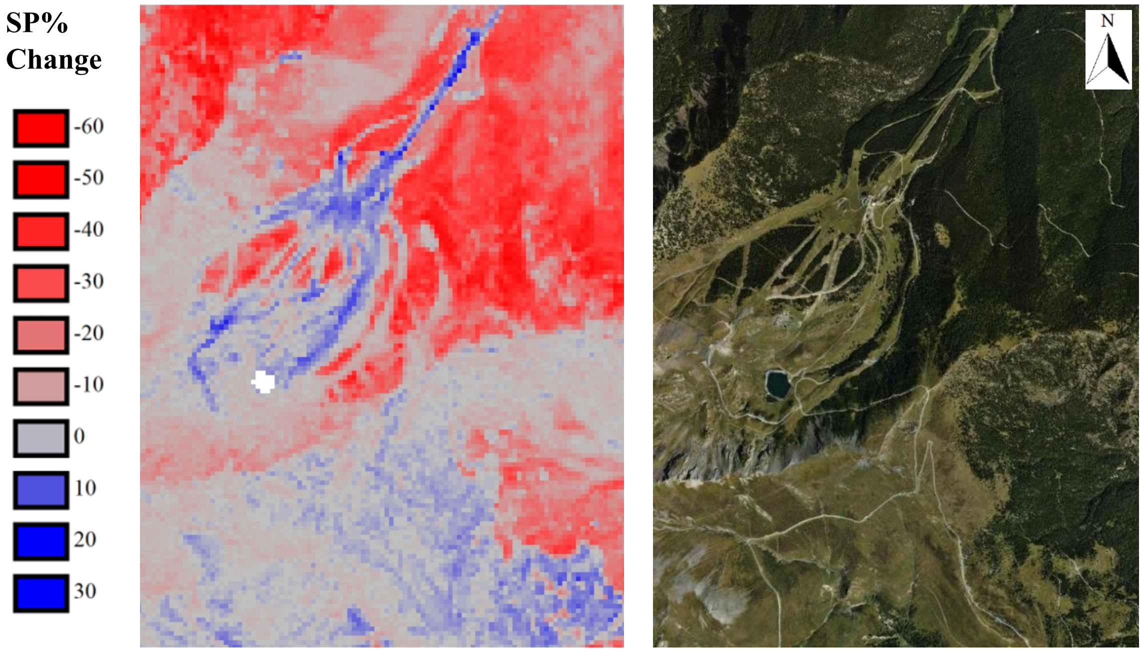

Figure A.8. Map of changes in SP % at the Espot ski resort, northeast of the Aigüestortes and Sant Maurici National Park, with a high-resolution orthophoto of the same area

Source: Own elaboration

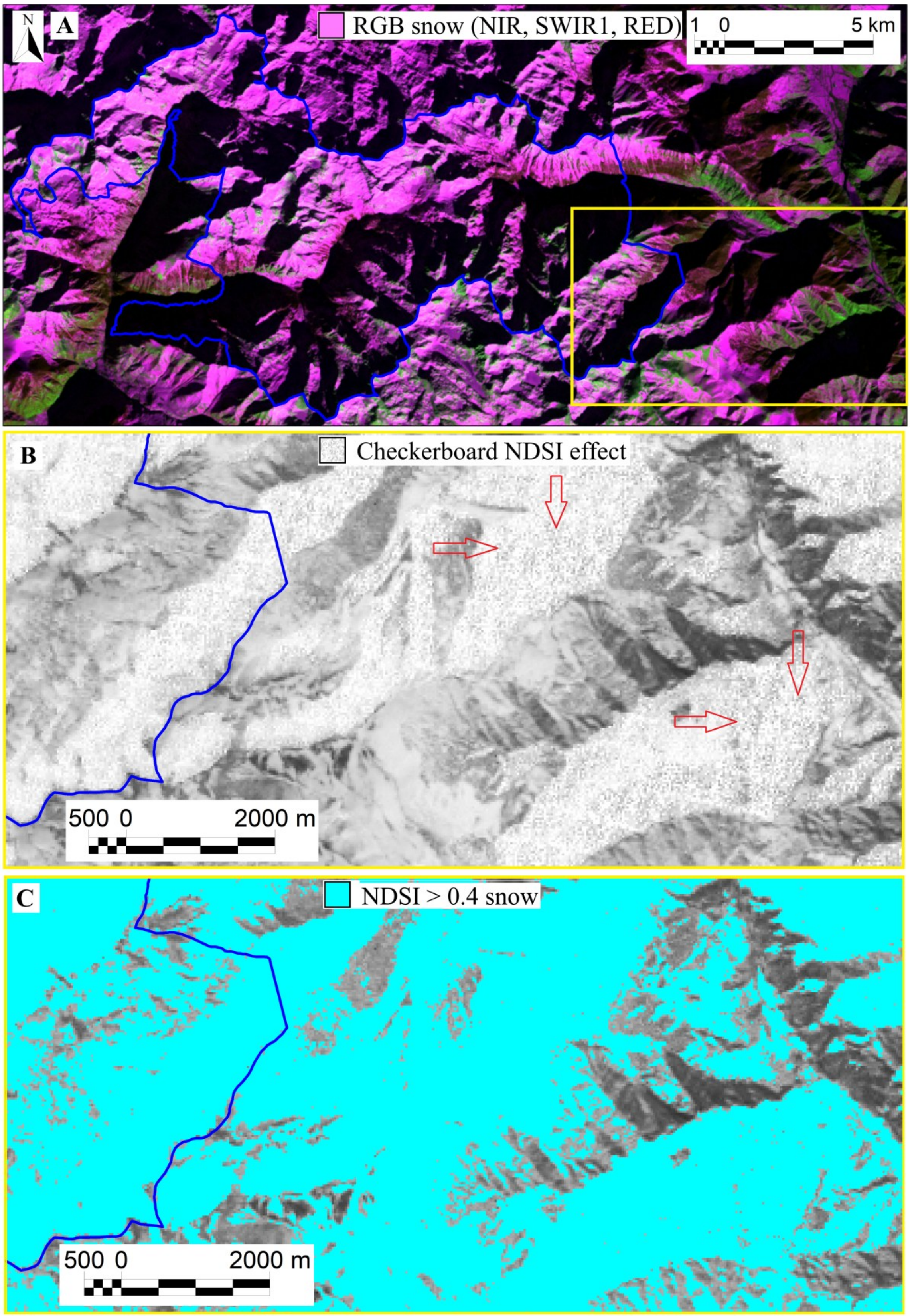

Figure A.9. Map of the National Park, December 20, 1990, Landsat-5. A: RGB (NIR, SWIR, Red); B: Detail of the NDSI in the southeast of the Park, checkerboard effect; C: Classification of snow with threshold 0.4 in the NDSI

Source: Own elaboration

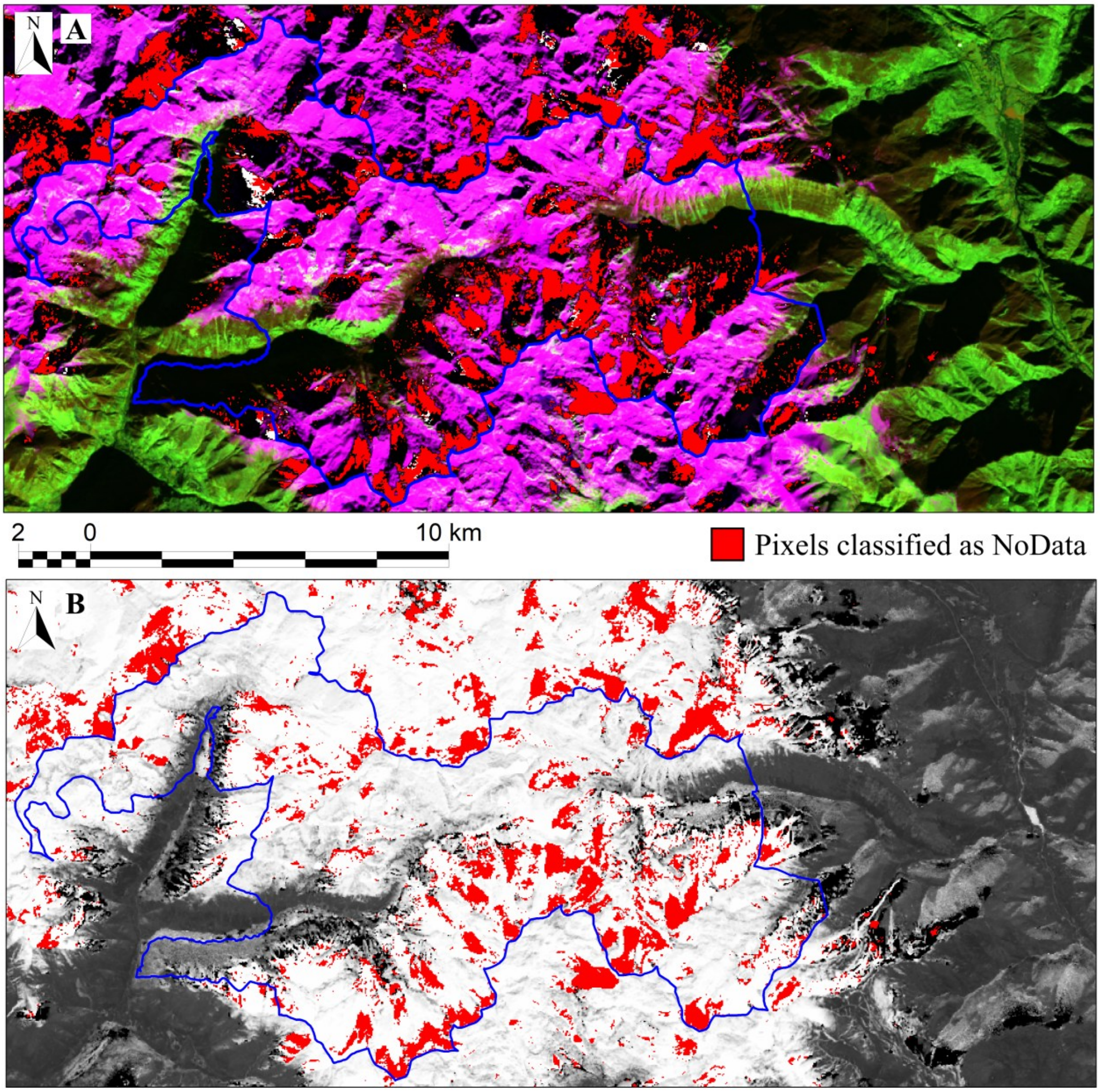

Figure A.10. Map of the National Park, December 22, 2014, Landsat-8. A: RGB (NIR, SWIR, Red); B: NDSI with most shaded areas classified as NoData
Source: Own elaboration